Article history: Received 8 November 2024, last revised 4 January 2025, accepted 4 January 2025



THE IMPACT OF A VORTEX GENERATOR ON A MIXTURE OF A JET WITH A MAINSTREAM FLOW OVER A FLAT PLATE

Nabeel Al-Zurfi

Asst. Prof., Department of Mechanical Engineering, Faculty of Engineering, University of Kufa, Al-Najaf, Iraq, Email: nabeelm.alzurfi@uokufa.edu.iq.

https://doi.org/10.30572/2018/KJE/160330

ABSTRACT

This work investigates the effects of adding vortex generators (VGs) in front of twin injection holes drilled on a flat plate geometry. To analyse the improvement of heat transfer, VGs are positioned at three different locations: 0D, D, and 3D upstream of the injection holes. The configurations used are prism-shaped VG of height = D, 1.5D, 2D, and 3D, with an inclination angle of 0° to 40°, and a blowing ratio of M=1.0. Using the commercial CFD code StarCCM+, the focus is on temperature distribution to examine the improvement of the injected jet coverage on the wall. The sst k-w turbulence model of the Reynolds-averaged Navier-Stokes method (RANS) is used to model the turbulent flow over a flat plate. The accuracy of the RANS approach to predict the jet in crossflow interaction (JICF) is evaluated in this study. The effective operation of this cooling enhancement is demonstrated by the region covered by the injected air along the flow direction. The results showed that the VG location is the crucial factor that controls the jet coverage. Compared to the base hole, the cooling performance produced by the VGs design exhibits obvious enhancement at all VGs locations. The jet footprint of the VG cases is larger than that of the base hole. Besides, it was also shown that the VG technique applied in the current research decreases the mixing process between the mainstream air and the secondary jet and enhances the coverage level. It was also found that the VGs generate strong reverse vortices moving against the main vortices, which destroys their undesirable effects and reduces the jet lift-off effect which then keeps the jet attached to the wall. In conclusion, the simulation results indicate a greater coverage area can be achieved when the VG is mounted at an upstream location too far from the injection hole.

KEYWORDS

Vortex generator, Film cooling, Turbulence flow, Jet interaction.



1. INTRODUCTION

By increasing the turbine inlet temperatures, high engine efficiency is expected in modern engines. The inlet temperatures of the high-pressure turbine are well above the acceptable material melting limits of the blades. Advanced cooling techniques such as internal cooling, external cooling, and thermal insulation coating are required to ensure the longevity of components. Film cooling, one of the external cooling technologies, is often used to protect the exposed external surfaces from the hot mainstream flows. To simplify, this kind of flow has been studied as a jet interacts with mainstream flows over a flat surface. During the interaction of a jet mixed with a cross flow (JICF), a stream of air is injected from a series of holes placed at several positions on the surface of a flat plate. Numerous critical flow and geometric parameters affect the behaviour of this interaction. In the last decades, a number of studies (Ito and Eckert, 1978; Andreopoulos and Rodi, 1984; Kelso and Perry, 1996) have been carried out on the region of a jet interacting with a cross-flow. Originally, a series of studies on the cylindrical injection hole were conducted to investigate the film cooling performance. It was discovered that counter rotating vortex pairs (CRVPs) form near the exit of the hole because of the strong mixing between the mainstream air and an injected air jet, the dynamics of which determine the mixing process. These CRVPs vortices are known to be the main cause of the sharp decline in film cooling efficiency and are detrimental to the cooling process.

The main disadvantage of the cylindrical holes is that their ability to improve film cooling performance is only partially realized when the values of the blowing ratio increase above the range of 0.5-1.0. Therefore, to meet the requirements of both ease of manufacturing and excellent film cooling performance, new shapes for injection holes and different configuration arrangements have been researched and created. Modifying the configuration around the hole is another way to weaken the CRVP, and the VG configuration is one of the approaches to achieve the desirable effect. VGs are flow control configurations that create fluid vortices that combine slower moving fluids near the wall with an external flow of greater momentum, minimizing or eliminating flow separation. Several researchers have focused their studies on creating secondary vorticity to reduce the effect of kidney vortex pairs. Khorsi et al. (2016) placed a crescent-shaped flow control device behind a cylindrical hole at different blowing ratios to improve film cooling efficiency. It was evident that the device significantly increased the effectiveness in the central part of the injection hole compared to the scenario without the device. The downstream VGs distribute the coolant jet laterally from the cylindrical hole as it flows over the top of the system.

Shinn and Vanka (2013) and Zaman et al. (2010) also conducted research using a delta VG. It

was discovered that the location of the VG can have a strong impact on how well the film cools. The film cooling performance of an upstream VG increases with increasing inlet distance. As VG distances increase, film cooling performance initially improves before deteriorating. Regarding the impact of the upstream distance on the cooling efficiency, it is observed that the influence of the rotational flow of the CRVP decreases as one moves further upstream of the VG. In another study, Delta VGs were positioned downstream of a series of film cooling holes by Rigby and Heidmann (2009). The results showed that using VGs to create beneficial downdraft vortices to suppress damaging updraft vortices was a very effective means of forcing coolant to the surface and spreading in the spanwise direction. Liu et al. (2013) investigated the performance of a coolant jet injected from a newly modified hole configuration. A crescentshaped block positioned downstream of a round hole using pressure-sensitive paint was studied. They found that the VG case had significantly better film coverage and higher performance of the film cooling than the non-VG case. They also found that as the blowing ratio increases near the hole, the laterally averaged effectiveness of film cooling decreases for all block heights. Similar findings were achieved in a study conducted by Zaman et al. (2010) on the question of how well a microramp VG placed downstream of a film hole works. They adjusted the height and position of the microramp VG and found that halving the height of the VG resulted in the jet lifting at a measurement point ten diameters from the aperture, which was ineffective. Conversely, the jet core was diffused when the VG height was doubled. They therefore concluded that the average height of 0.75 D was best suited to keep the jet close to the wall without causing large power dissipation. The authors also reported that the flow field at the measurement point was not significantly affected by moving the VG up to three diameters from the hole.

Furthermore, Deng et al. (2022) used different configurations of winglet-VG pairs with a height of 0.4D positioned in front of the injection hole using a Reynolds Averaged Navier Stokes equations (RANS) method. The effectiveness reduced as the blow ratio was increased from Br = 0.5 to 1.5, with a rapid decrease from Br = 1.0 to 1.5. However, all shapes achieved better film coverage than the non-VG case. Zheng et al. (2021) investigated the effect of placing a microramp VG in front of the hole at different heights, blowing ratios, and locations using PIV on the efficiency of film cooling. They proved that the effectiveness of film cooling decreased with the decrease in the height of VG at a relatively low blow ratio. However, at relatively low injection ratios, the height difference is noticeable, and at relatively high injection ratios (Br = 0.8) it becomes even more noticeable. They also claimed that the height of the VG is more important to the effectiveness of film cooling than the location of the VG. He and Feng

(2021) carried out a RANS study to investigate the influence of adding a V-shaped VG design upstream of an injection hole with different heights and blowing ratios on cooling efficiency. The authors found that at all tested heights (H/D = 0.05, 0.10, 0.15, 0.20, 0.25), the effectiveness of film cooling decreased when the blowing ratio of Br = 0.50 was increased to 1.50. Furthermore, they claimed that effectiveness is significantly affected by the height of the VG, with higher height resulting in better film cooling effectiveness over the entire range of blowing ratios tested. Zhang et al. (2020) examined a new design that combine the VG with a shaped hole geometry. Their study included different configurations to examine the performance of shaped hole geometry. The results showed that the shaped hole configuration produced a higher cooling performance than the other models at all blowing ratios.

On the other hand, a large eddy simulation technique was used by Zhao et al. (2022) to investigate vortex generators of delta winglets pairs on the film hole with the compound angle at the blowing ratio of 1.0. Their results showed that the vortex generator improves significantly the cooling performance. More recently, a computational and experimental study was conducted by Straub et al. (2024) to examine the effect of a vortex generator placed downstream of the cylindrical hole on the performance of film cooling design. It was found that the downstream vortex generator was able to enhance the film cooling effectiveness by 150 % higher than that of the case without the vortex generator at higher values of blowing ratio. Additionally, Halder (2025) examined experimentally the impact of the VG system on the cooling performance. He found that the cooling performance increased as the VG was placed closer to the film hole.

According to the literature review, cylindrical holes are the easiest and least expensive to manufacture and maintain. Since they also produce lower aerodynamic losses than, for example, shaped holes, they ensure constant cooling performance. Thus, the main aim of this study is to investigate how VGs design improves the jet coverage area produced by the cylindrical holes. The harmful kidney vortex created by the main hole is offset by the anti-vortex vortices created by the VG system, which ensures that the jet sticks to the wall. However, the search for the best, most effective, and useful VGs is still ongoing. According to all the above studies, the geometric parameters of the VG can significantly affect the flow pattern and the performance of the cooling strategy. However, it is still unclear how the height, position, and other geometric parameters of the VG interact. Therefore, the present study is carried out to improve our understanding of the mechanism by which VGs improve cooling technology, as well as examine the effects of height and distance of different cases of VG configurations at low blowing ratios. Furthermore, the degree of enhancement of the cooling technique due to

the use of the VG design is presented and discussed. The findings of such studies will help to understand the physical phenomena related to the jet and cross-flow interaction and be beneficial in designing a more efficient cooling system.

2. MATHEMATICAL FORMULATION

The incompressible, steady-state, turbulent flow, and three-dimensional continuity, momentum, and energy equations are solved to determine the flow and heat transfer characteristics of this study. The governing and transport equations (Versteeg and Malalasekera, 2007) are based on these hypotheses.

$$\frac{\partial}{\partial \mathbf{x}_{i}}(\rho \mathbf{u}_{i}) = 0 \tag{1}$$

$$\frac{\partial}{\partial x_{i}} (\rho u_{i} u_{j}) = -\frac{\partial p}{\partial x_{i}} + \frac{\partial}{\partial x_{j}} \left[(\mu + \mu_{t}) \left(\frac{\partial u_{i}}{\partial x_{i}} + \frac{\partial u_{j}}{\partial x_{i}} \right) \right] - \frac{2}{3} \frac{\partial}{\partial x_{j}} \rho k \delta_{ij} + S_{\emptyset i}$$
 (2)

$$\frac{\partial}{\partial x_{i}}(\rho T u_{i}) = \frac{\partial}{\partial x_{i}} \left[\left(\frac{\mu}{Pr} + \frac{\mu_{t}}{Pr_{t}} \right) \frac{\partial T}{\partial x_{i}} \right]$$
(3)

The Menter $k-\omega$ SST turbulence model was used in this study to calculate the turbulent eddy viscosity (μ_t), as follows (Versteeg and Malalasekera, 2007):

$$\frac{\partial}{\partial x_{i}}(\rho k u_{i}) = \frac{\partial}{\partial x_{i}} \left[\left(\mu + \frac{\mu_{t}}{\sigma_{k}} \right) \frac{\partial k}{\partial x_{i}} \right] + 2\mu_{t} \delta_{ij} \cdot \delta_{ij} - \frac{2}{3} \rho k \frac{\partial u_{i}}{\partial x_{j}} \delta_{ij} - \beta_{1} \rho k \omega \tag{4}$$

$$\frac{\partial}{\partial x_{i}}(\rho \omega u_{i}) = \frac{\partial}{\partial x_{i}} \left[\left(\mu + \frac{\mu_{t}}{\sigma_{\omega 1}} \right) \frac{\partial \omega}{\partial x_{i}} \right] + \gamma \left(2\rho \delta_{ij} \cdot \delta_{ij} - \frac{2}{3} \rho \omega \frac{\partial u_{i}}{\partial x_{j}} \delta_{ij} \right) - \beta_{2} \rho \omega^{2} + 2 \frac{\rho}{\sigma_{\omega 2} \omega} \frac{\partial k}{\partial x_{k}} \frac{\partial \omega}{\partial x_{k}} \tag{5}$$

The turbulent eddy viscosity is defined as: $\mu_t = \rho k/\omega$.

The values of the blowing ratio are one of the main parameters in the JICF study. It is defined as follows (Ajersch, 1997):

$$M = \frac{\rho_c u_c}{\rho_\infty u_\infty} \tag{6}$$

Where ρ_c and u_c are the density and velocity of the jet at the inlet of the hole, respectively.

Furthermore, to characterize the performance of film-cooling, the effectiveness (η) can be calculated from the values of temperature as follows (Ajersch, 1997):

$$\eta = \frac{T_{\infty} - \langle T_{aw} \rangle}{T_{\infty} - T_c} \tag{7}$$

where T_{∞} is the temperature of mainstream air, T_c is the temperature of the injected air, and T_{aw} is the flat plate surface adiabatic wall temperature.

In the current research, the spanwise-averaged film-cooling effectiveness ($\bar{\eta}$) was used as the main parameter in representing the performance of film cooling and was defined as (Ajersch, 1997):

$$\overline{\eta} = \frac{\sum_{i=1}^{n} \eta_{i} A_{i}}{\sum_{i=1}^{n} A_{i}}$$
 (8)

In Eq.8, the sample (n) represents the node number used in the spanwise direction at a certain streamwise location.

3. PHYSICAL MODEL

The main flow domain with different configurations of vortex generators (VGs) and two inlet cooling pipes is created by using the StarCCM+ code. Fig. 1 and 2 show the main flow domain. The dimensions of this block are L=10D, W=5D, and H=6D.



Fig. 1 The computational domain geometry Fig. 2 Side view of the computational domain

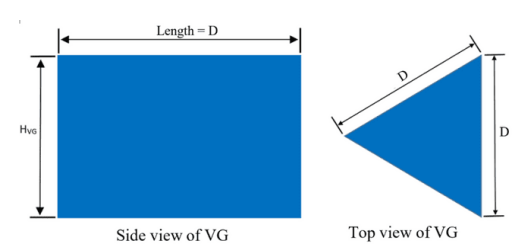


Fig. 3 Prism-shaped VG design of HVG =D, 1.5D, 2D, and 3D

To simulate the jet with a cross-flow interaction, one row of injection holes is positioned on the flat plate surface. This row includes only two round holes with a diameter of D = 5 mm and spanwise spacing of 15 mm (P/D=3.0). The length of the hole pipe is 10 cm which gives a length-to-diameter ratio of L/D=20. The pipe formed an angle of 45° with the streamwise direction.

A pair of vortex generators are installed in front of each injection hole. It is known that vortex generators can produce anti-counter rotating vortex pairs (ACRVP), which have an impact on the jet coverage. VG designs are being tested at three locations and three different heights of H_{vg} =D, 1.5D, 2D, and 3D. Fig. 3 shows the prism-shaped VG design.

The top-tilted VG design as shown in Fig.4 has four different tilt angles of 0°, 10°, 20°, and 40°.

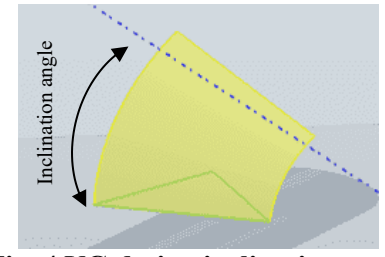


Fig. 4 VG design inclination angle

These vortex generators are placed in front of each hole. Three different locations of VG position 0D, D, and 3D from the hole are also investigated. Their configurations are shown in Fig. 5.

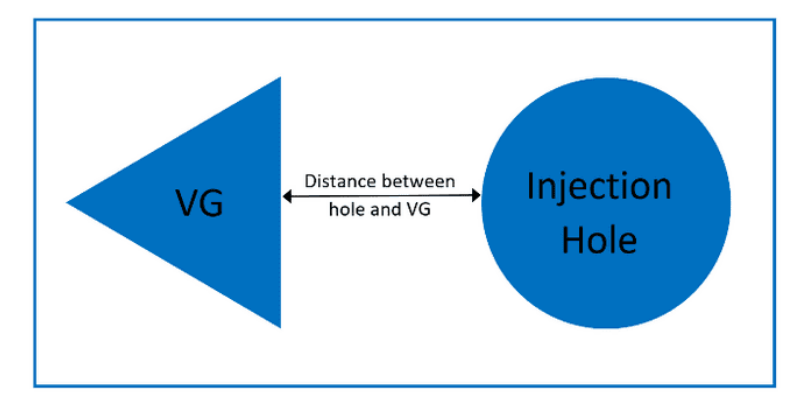


Fig. 5 Location of vortex generator upstream of the hole

4. BOUNDARY CONDITIONS

The mainstream inlet temperature (T_{∞}) and velocity (u_{∞}) are 300 K and 18 m/s, respectively. At the mainstream inlet, a turbulence length scale of 3.0 % of the geometry length and a turbulence intensity of 5 % are applied. With a static pressure of P_{out} =101.325 Kpa, the flow outlet boundary condition is configured as a pressure outlet. The symmetry planes are subject to a periodic flow boundary condition. To shield the plate surface from the hot main flow, comparatively cool air is used as a secondary flow. The air is injected directly into the hole pipe inlet section with a blowing ratio of M=1.0. Since the density ratio of the secondary flow to mainstream flow is DR =1.7, the injected air temperature (T_c) is assumed to be 262 K. The surfaces of the flat plate and injection holes are subject to adiabatic no-slip conditions.

Furthermore, the simulations were carried out with different secondary and mainstream jets inlet temperatures, which have a great influence on the hydrodynamic behavior of the proposed problem. The temperature differences may lead to fluctuations in air properties, especially in the region when the injected air gets mixed with the mainstream flow. To capture the spatial variation of the air properties flowing over the flat plate, the dynamic viscosity, thermal conductivity, and fluid density were expressed as a function of temperature using Sutherland's laws and the ideal gas law for an incompressible flow.

The finite volume approach was used to discretize the governing and transport equations in conjunction with the SIMPLE algorithm scheme for the velocity coupling (Alhusseny et al., 2023) proposed by Patankar and Spalding (Patankar and Spalding, 1972). The convection terms of the governing equations were discretized using the first-order upwind scheme while the diffusion terms were discretized using the first-order central scheme (Alhusseny et al., 2023).

5. GRID GENERATION

Using starccm+ software, two multiblock grids were created: one covering the flat plate region Fig. 6 (a and b), and the second one covering the region inside the injection holes Fig 6 (c). Polyhedral with prism layer grids formed the entire flat plate region. On the flat plate, the prism layer meshes are adjusted so the mesh becomes clustered near the wall as shown in Fig. 6 (b). At a stretching ratio of 1.3, the mesh was separated from the viscous wall. To accurately represent the interface area, an initial height of 0.0196 mm was used.

In contrast, in the second domain, there were two pipes of injection holes as shown in Fig.6 (c). The two-block grids were then combined to create a "hybrid" mesh with a non-compliant interface boundary. For simulation accuracy, the value of two adjacent mesh sizes in each direction was kept between the ranges from 0.81 to 1.2. Seven different grid topologies were examined in this study to investigate the system grid-independent solution. The numbers of examined meshes were 0.5 M, 1.0 M, 1.5 M, 2.0 M, 2.5 M, 3.0 M, and 3.5 M. As a result, the number of cells with approximately 3,000,000 cells were selected for the entire system.

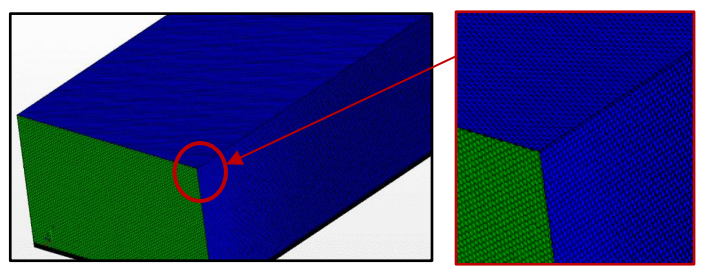
6. VALIDATION STUDY

The baseline cylindrical hole (CH) model of the experimental study of Zhang et al. (2020) is used to verify the current numerical model. Such problems require precise numerical simulations to accurately predict the jet-cross-flow interaction. Because of the intrinsic complexity and sensitivity of the jet with a cross-flow interaction, the RANS approach is typically unable to accurately capture the flow field and heat transfer. In particular, as shown in Fig. 7, RANS models are unable to predict flow separation and vortex interaction immediately downstream of the hole.

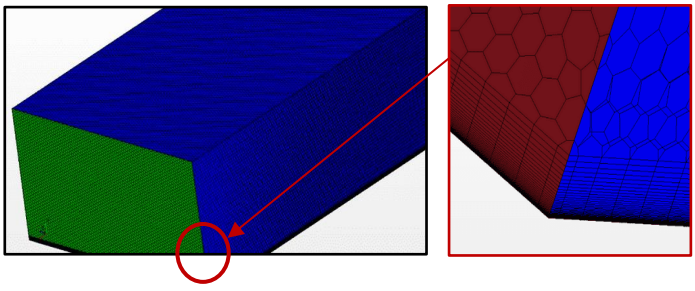
However, after x/D = 3.0, the model remains reasonably accurate and accurately predicts the trend of laterally averaged effectiveness. Fig. 8 shows the qualitative comparison between the experimental and computational results using contour plots of the effectiveness.

7. RESULTS AND DISCUSSION

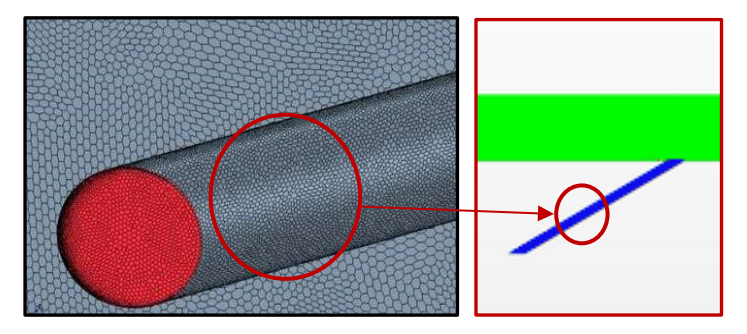
The impact of the VG design placed upstream of the injection holes at M=1.0 is systematically shown in the cooling performance of different configurations at three different locations. To improve the cooling efficiency, this article explores the addition of a VG system at the upstream position of each hole. The contour diagram illustrating the flow mechanism of temperature distributions is presented in different views in this section. The distribution of lateral-averaged film cooling effectiveness is also displayed and discussed.



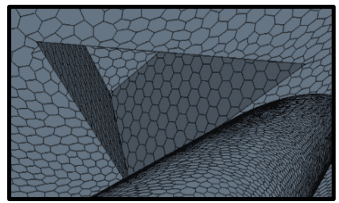
a- The main simulated block (flat plate domain with polyhedral meshes)



b- The main simulated block (flat plate domain with Prism layers meshes near the flat plat wall)



c- The second simulated block (injection hole pipe domain with polyhedral meshes)



d- The main simulated block (Vortex generator geometry with polyhedral meshes) Fig. 6 Grid structures for the system with VG design

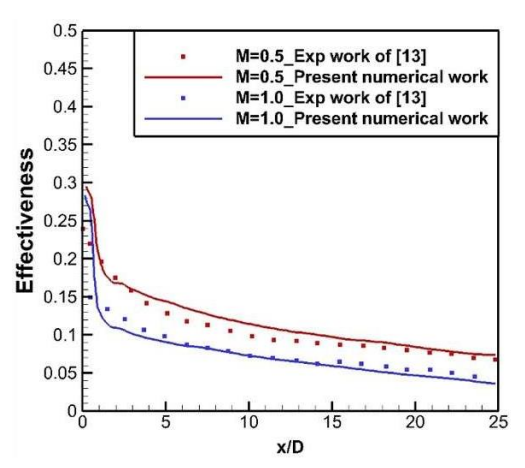
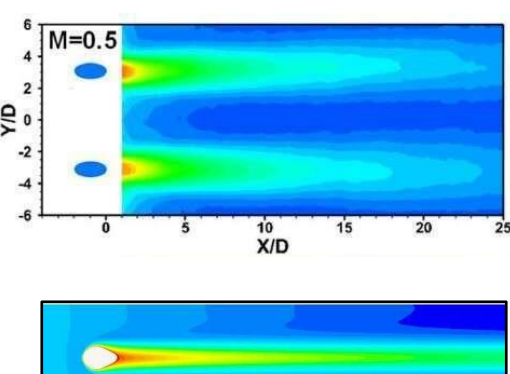


Fig. 7 CFD model validation: effectiveness



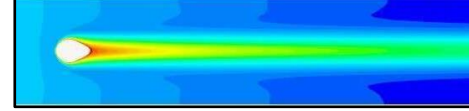


Fig. 8 CFD model validation: contour plot

7.1. Temperature distribution.

Fig. 9 illustrates the temperature distributions at a blow ratio of 1.0 with heights of D, 2D, and 3D. The VG systems are positioned at three different distances from the holes: 0D, D, and 3D. It should be noted that the contour diagram takes into account the jet coverage on the surface of the plate itself and therefore does not take into account the location of the VG or injection holes.

A larger coverage area of coolant air can be seen in Fig. 9 when a VG is added. It is believed that the main cause of the sharp decline in the covered area is the counter-rotating vortices pairs (CRVPs) produced by the JICF. The ability of the cooling air to provide thermal protection is quickly destroyed as these vortices entrain the main flowing air and push it toward the wall. Thus, the anti-countering rotating vortex pairs (ACRVPs) generated by VG systems mitigate the impact of the CRVPs and thus reduce the jet lift-off effect. Reducing the effect of lift-off phenomena keeps the coolant jet closer to the wall which improves the coverage area as shown in Fig. 9.

Changing the VG height also affects the coverage area, as shown in this figure. The jet coverage in Fig. 9 (1d) is better than that in Fig. 9 (1b and c). Increasing the height of VG leads to generating stronger (ACRVP) which has a considerable impact on the main vortices. The other two shorter heights create a blur effect, the area directly behind the hole has a noticeable jet coverage. The VGs are then positioned at D distance from the holes. Fig. 9 (2) shows that a higher VG provides a larger coverage area in the flow direction. Fig. 9 (3) shows that the jet coverage increases significantly when the VG is moved to a further distance of 3D. In this case, the ACRVPs will have enough time to build up and become stronger. In Fig. 9 (3b), a VG height of 3D can produce a bigger region of coolant coverage along the streamwise compared to D and 2D as shown in Fig. 9 (3c) and Fig. 9 (3d). In contrast, they produce higher effectiveness in the region further downstream of the holes. A larger height results in a larger recirculation area, resulting in more significant entrainment of cross-flow fluid into the wake of the jet.

Fig. 10 shows the results of the VGs design with three different inclination angles of 10°, 20°, and 40° to the streamwise direction. At a distance of 0D from the injection hole, VGs with the three inclination angles are shown in Fig.10 (1). Comparing the coverage areas produced by the VGs in Fig. 10 (1b, c, and d), the VGs with the inclination angles of 20° and 40° both provide funnel-shaped coverage in the region immediately behind the hole while VG with 10° provides the greatest coverage area in both stream and spanwise directions. The reason for this behaviour is that the VG with a higher angle pushes the ACRVPs in the Y direction which reduces its impact on the main vortices. Although VG with 40° provides longer and more comprehensive

coverage than VG with 20° , however, 20° VG provides greater coolant coverage in the area downstream of the hole. This is due to the smaller circulation and separation region caused by the 20° VG.

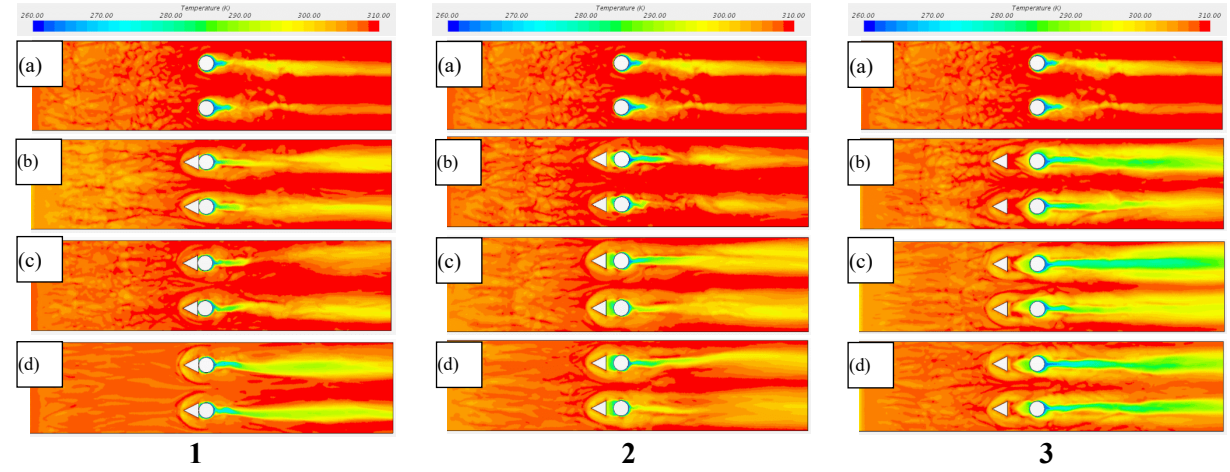


Fig.9 Temperature distributions with a distance of (1) 0D, (2) D, and (3) 3D upstream of the injection holes at different height of VG: (a) no VG, (b) D, (c) 2D, and (d) 3D.

Furthermore, the VGs are shifted to a distance of D away from the hole as shown in Fig.10 (2). The efficiency of the cooling process becomes much more apparent due to increasing the strength of the ACRVPs. In Fig. 10 (2b), 10° VG still generates the bigger total area of jet coverage. Fig. 10 (2c and d) shows that 10° and 20° VGs provide a funnel-shaped jet cover immediately behind the injection hole. The jet coverage is the biggest at 20° VG, but the coverage ends earlier than at that of 40° because the 40° VG produces weaker ACRVPs so the main vortices reduce the coverage area immediately downstream of the hole and then due to the flow acceleration caused by the VG, the flow reattached further downstream of the hole. The same behaviour was seen for VG placed at the location of 3D as shown in Fig.10 (3).

7.2. Coolant contour

The prism VG cross-sectional contour with a blow ratio of 1.0 is shown in Fig.11. In this case, there is no VG as shown in Fig.11 (1a). At X/D=2 the jet cover begins to form. The entire jet was lifted above the flat plate surface as the CRVP began to form at X/D=4. Furthermore, the entire jet is lifted at X/D=8 without coming into contact with the surface. As seen in Fig. 11 (1b and c) at the streamwise location of X/D=8, the CRVP is still influencing the jet coverage by raising it, even though the VGs, as shown in both figures, aid in flattening the jet coolant and creating a wider coverage. The ACRVP has begun to form at X/D=4, and it is stronger with a VG high of 2D as seen in Fig.11 (1d). The ACRVP opposes the CRVP and then reduces its effect. At X/D=8, the entire ACRVP shape is formed. However, because of the effectiveness of ACRVP and the insufficient distance of VG from the hole, the jet is still not very firmly adhered to the surface.

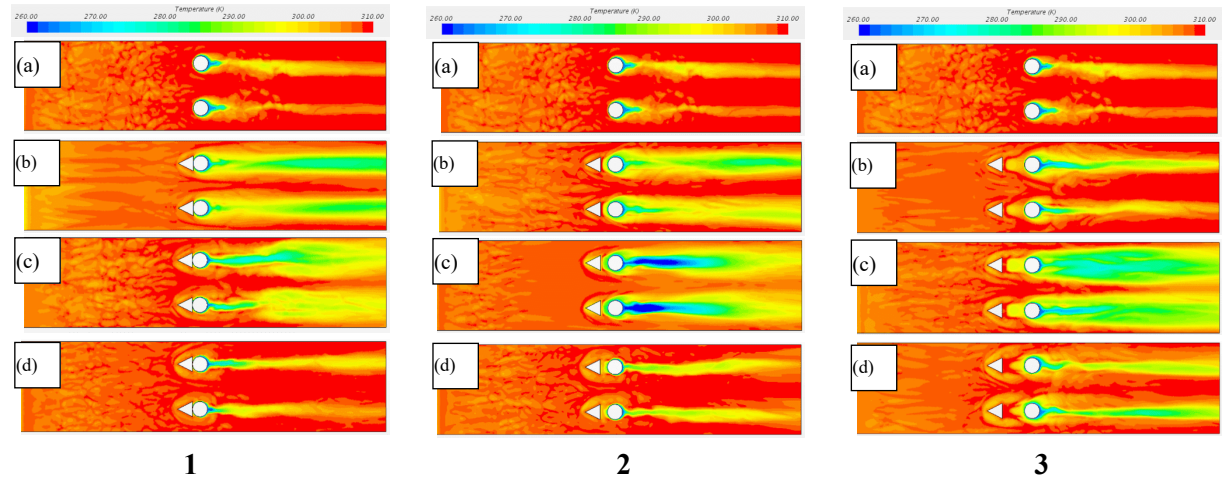


Fig. 10 Temperature distributions with a distance of (1) 0D, (2) D, and (3) 3D upstream of injection holes at different inclined angles of VG: (a) no VG, (b) 10°, (c) 20°, and (d) 40°.

The performance of the VG with a height of D at a distance of D upstream of the injection hole as shown in Fig. 11 (2b) is comparable to that of Fig. 11 (1b) at a distance of 0D. Fig. 11 (2c) shows the trend from X/D=0 to X /D=8 compared to Fig.11 (1c). They are quite similar, but in this case, the air jet is flatter, more stable, and more uniform in shape at a distance of D. The jet in Fig.11 (2d) is influenced by the ACRVP produced by VG of the height of 2D placed at a distance of D upstream of the hole. Comparing this case to a distance of 0D, the shape is wider and more uniform, and the jet adheres much more strongly to the surface. This behaviour is because as the VG is placed further away from the hole, the ACRVP gets stronger as it is moving toward the hole making the CRVP weaker which reduces the lift-off effects. Fig.11 (3a and b) shows that the CRVP produced by VGs with the height of D and 2D still influences the jet coverage area. In Fig.11 (3d), it is seen that increasing the VG height to 2D can lead to strengthening the effect of the ACRVP. Unlike 0D and D, all cases with a distance of 3D are found closer to the surface. This indicates that better coverage has been achieved.

Fig.12 displays the results of the VG system with three different inclination angles. The ACRVP produced by 10° VG is still weaker than the CRVP, although it can bring the coolant jet closer to the plate surface (see Fig.12 (1b)). Thus, CRVP remains visible at X/D=8. The 20° VG in Fig.12 (1c) can produce a strong ACRVP. The jet remains partially detached from the surface at X/D=8, although the jet coolant coverage increases downstream. In Fig.12 (1d), at X/D=8, a large and wide pair of vortices is visible, and the ACRVP becomes much stronger as X/D increases. However, the jet cannot adhere to the surface.

The coolant coverage area with the VG placed at a D distance is comparable to that at 0D as shown in Fig.12 (2). In the case when VG is inclined with 10°, the CRVP is seen to be stronger; however, it becomes weaker when using a VG with 20° and 40°. The 10° inclined VG case in

Fig.12 (3b) has a comparable performance to the other two distances. The 20° tilted VG case can maintain a wide spread and flattening of the jet coolant as shown in Fig.12 (3c). When X/D is increased, the effect is significantly better. The ACRVP made the coolant jet stronger and wider as shown in Fig.12 (3d), but is not strong enough to keep the air jet closer to the surface.

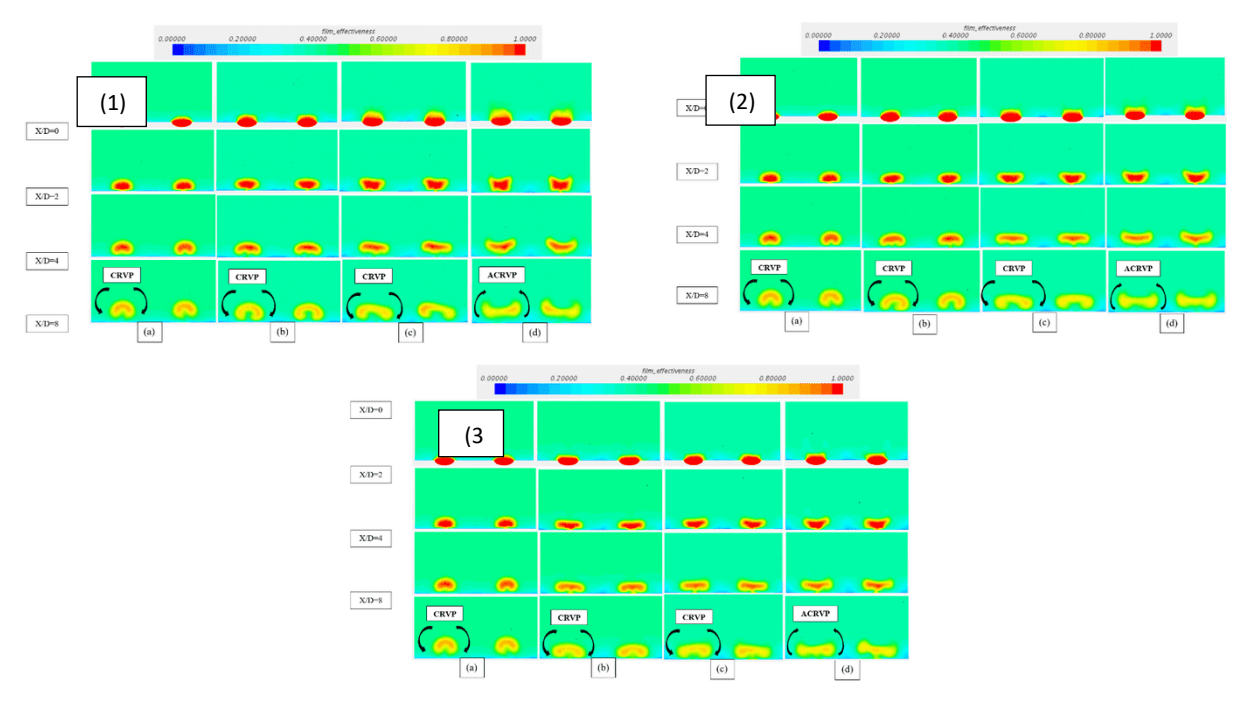


Fig. 11 Jet cooling contour with a distance of (1) 0D (2) D, and (3) 3D upstream of the injection holes at different heights of VG: (a) no VG, (b) D, (c) 2D, and (d) 3D.

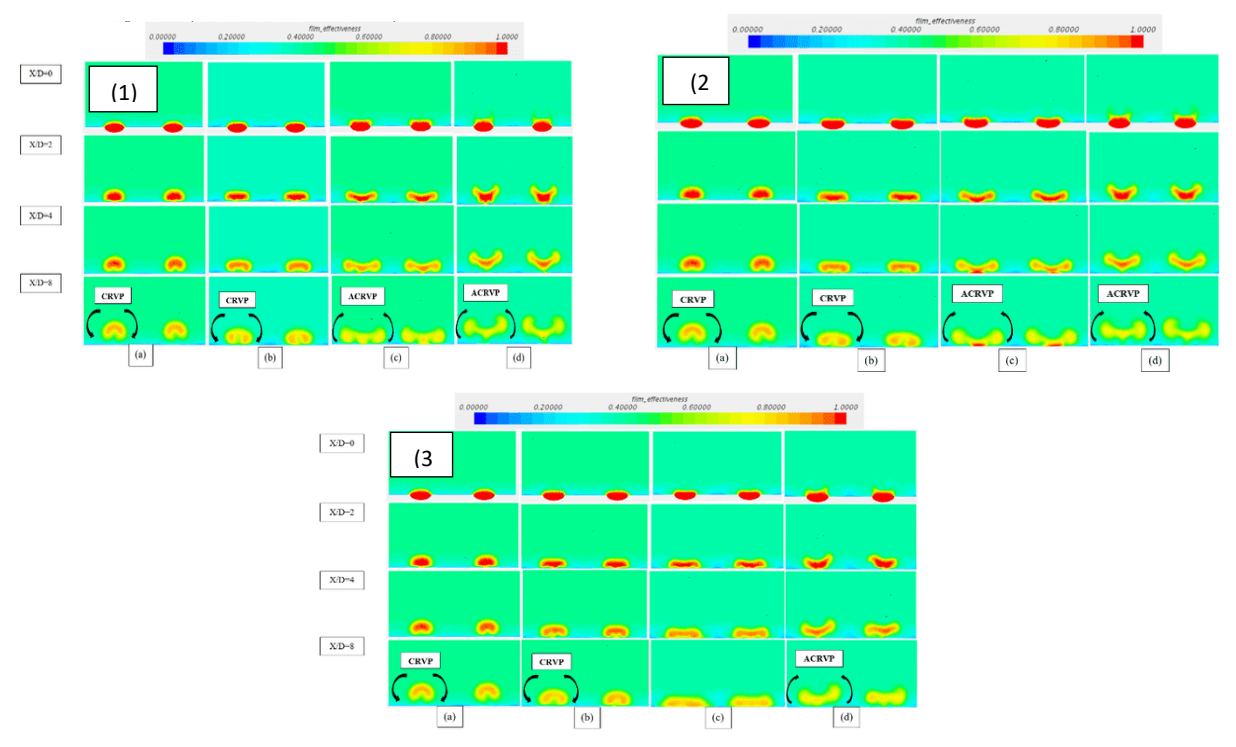


Fig.12 Jet cooling contour with a distance of (1) 0D, (2) D, and (3) 3D upstream of the injection holes at different inclined angles of VG: (a) no VG, (b) 10°, (c) 20°, and (d) 40°.

7.3. Spanwise-averaged film cooling effectiveness.

The spanwise-averaged distributions of the effectiveness for all VGs at a blowing ratio of 1.0 are shown in Figs 13 and 14. Fig.13 compares the cooling efficiency of the base round hole and VG cases. This figure shows that for both the base case and VG cases, the effectiveness of cooling decreases rapidly with increasing x/D. For the base case, the effectiveness near the hole exit reaches a high value and then decreases rapidly until it reaches x/D=4.0 and then begins to increase gradually. The jet lift-off effect is the cause of the decrease in cooling efficiency near the jet exit. The jet separates and the main flow enters the area behind the jet exit, resulting in insufficient surface coverage.

For the VG cases, the generated ACRVP moves above the injected jet from the hole and works as a fluid barrier against the mainstream air. Besides, it fills the low pressure region of the air jet and mitigates it to move attached to the wall.

The cooling effectiveness of all VG cases in Fig.13 is performing better than that of the case without VG. The effectiveness of the VG cases continues to rise until the edge of the plate is reached except for that of VG with a height of D where it decreases aft x/D=15.0. This behaviour is because of the effect of the ACRVP which cancels the effect of the main CRVP. This leads to weakening the lift-off effect and thus keeps the coolant jet attached to the surface. It is seen that prism VGs significantly improve the cooling performance when positioned at the 3D upstream of the holes as shown in Fig.13c. As the VGs placed away from the hole, the ACRVP will have the time to grow and then become stronger. As the ACRVP becomes stronger, the CRVP becomes weaker which means less effect of jet-lift off. The case of VG paced at 1.5D, has a value more than twice that without VG, and offers incredibly a good performance.

In Fig.14a, excellent performance is achieved in the case of a 20° inclined VG, followed by a 10° inclined VG. This phenomenon is due to that 20° inclined VG can create ACRVP and this angle keeps them closer to the surface so they are able to reach the CRVP and destroy it before it causes the jet lift-off.

On the other hand, since it has the same values of cooling effectiveness compared with that of no VG, the 40° tilted VG has almost no effect. They have almost identical curves. A VG tilted at 20° maintains its performance in Fig.14b, followed by a VG tilted at 10°. This time a 40° tilted VG works slightly better than no VG. 40° inclined VG creates ACRVP as the other VGs cases but unfortunately, the generated vortices are lifted away from the surface due to the high inclination angle which reduces their impact on the main vortices.

In Fig. 14c, the VG inclined at 20° performs better at a distance of 3D upstream of the hole. Its cooling efficiency is almost four times higher than that of no VG case. However, the VG with an inclination of 10° falls along the main flow direction, while the VG with an inclination of 40° performs significantly better at this distance.

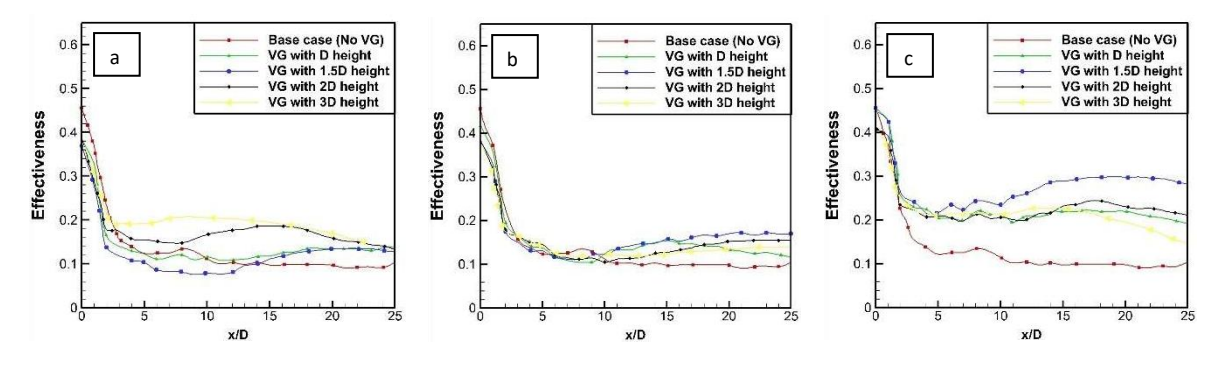


Fig.13 Spanwise-averaged effectiveness of different VG cases with a distance of (a) 0D, (b) D, and (c) 3D.

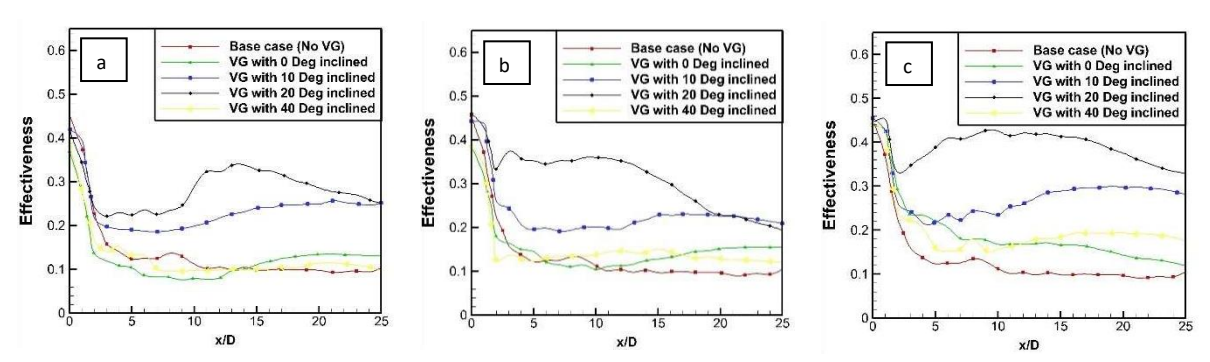


Fig.14 spanwise-averaged effectiveness of different VG cases with top tilted surface with distance of (a) 0D, (b) D, and (c) 3D.

8. CONCLUSIONS

In this study, an innovative VG model is used. The effectiveness is measured at a blowing ratio of M=1.0. The following are the main conclusions:

- 1- The jet coverage is improved by the use of the VG technique in both the lateral and downstream directions of the injection holes. The jet footprint becomes wider and larger by nearly 150 200% compared with that of the base case.
- 2- The maximum jet coverage is achieved with a VG inclined by 20°. The effectiveness values are higher by 50-100 % than other configurations.
- 3- The key to suppressing the CRVP is ACRVP, and the strongest ACRVP is found in prisms VG at 1.5D and 2D heights at a distance of 3D. The strongest ACRVP is produced by 20° tilted VG, which can both suppress the CRVP and flatten it to provide larger coverage.
- 4- The highest value of the lateral-averaged effectiveness is reached at a value of η =0.43 by 10° and 20° inclined VGs at 3D distance.

5- In terms of jet coverage area and lateral-averaged effectiveness, the tilted vortex generator exhibits better tend than a normal VG; however, the angle of inclination must not be too large. The ideal configuration has an angle of around 20°.

9. REFERENCES

Ajersch, P. et al., (1997). Multiple jets in a crossflow: Detailed measurements and numerical simulations. Journal of Turbomachinery, 119(2), pp.330–342. https://doi.org/10.1115/1.2841116.

Alhusseny, A. et al., (2023). A porous media approach for numerical optimisation of thermal wheel. Kufa Journal of Engineering, 14(4), pp.56–68. https://doi.org/10.30572/2018/KJE/140405.

Alhusseny, A. et al., (2023). Graphite foam structures as an effective means to cool high-performance electronics. Kufa Journal of Engineering, 15(2), pp.39–60. https://doi.org/10.30572/2018/KJE/150204.

Andreopoulos, J. and Rodi, W., (1984). Experimental investigation of jets in a crossflow. Journal of Fluid Mechanics, 138, pp.93–127. https://doi.org/10.1017/S0022112084000057.

Deng, H. et al., (2022). Overall cooling performance evaluation for film cooling with different winglet pairs vortex generators. Applied Thermal Engineering, 201, 117731. https://doi.org/10.1016/j.applthermaleng.2021.117731.

Halder, N., (2025). Experimental investigation on vortex generator's distance from film cooling hole. Journal of Thermal Science and Engineering Applications, 17(1), 011006. https://doi.org/10.1115/1.4066985.

He, J., Deng, Q. and Feng, Z., (2021). Film cooling performance enhancement by upstream v-shaped protrusion/dimple vortex generator. International Journal of Heat and Mass Transfer, 180, 121784. https://doi.org/10.1016/j.ijheatmasstransfer.2021.121784.

Ito, S., Goldstein, R.J. and Eckert, E.R.G., (1978). Film cooling of a gas turbine blade. Journal of Engineering for Power, 100(3), pp.476–481. https://doi.org/10.1115/1.3446382.

Kelso, R.M., Lim, T.T. and Perry, A.E., (1996). An experimental study of round jets in cross-flow. Journal of Fluid Mechanics, 306, pp.111–144. https://doi.org/10.1017/S0022112096001255.

Khorsi, A., Guelailia, A. and Hamidou, M.K., (2016). Improvement of film cooling effectiveness with a small downstream block body. Journal of Applied Mechanics and Technical Physics, 57(4), pp.666–671. https://doi.org/10.1134/S0021894416040106.

Liu, B., An, J., Zhang, C. and Zhou, S., (2013). Film cooling of cylindrical hole with a downstream short crescent-shaped block. Journal of Heat Transfer, 135(3). https://doi.org/10.1115/1.4007879.

Patankar, S.V. and Spalding, D.B., (1972). A calculation procedure for heat, mass and momentum transfer in three-dimensional parabolic flows. International Journal of Heat and Mass Transfer, 15(10), pp.1787–1806. https://doi.org/10.1016/0017-9310(72)90054-3.

Rigby, D.L. and Heidmann, J.D., (2009). Improved film cooling effectiveness by placing a vortex generator downstream of each hole. Turbo Expo: Power for Land, Sea, and Air, Paper No: GT2008-51361, pp.1161–1174. https://doi.org/10.1115/GT2008-51361.

Shinn, A.F. and Vanka, S.P., (2013). Large Eddy Simulations of film-cooling flows with a micro-ramp vortex generator. Journal of Turbomachinery, 135(3). https://doi.org/10.1115/1.4006329.

Straub, D. et al., (2024). Effects of downstream vortex generators on film cooling a flat plate fed by crossflow. Journal of Turbomachinery, 146(5), 051011. https://doi.org/10.1115/1.4064316.

Versteeg, H.K. and Malalasekera, W., (2007). An Introduction to Computational Fluid Dynamics: The Finite Volume Method. 2nd ed. Harlow: Pearson Education.

Zaman, K.B.M.Q., Rigby, D.L. and Heidmann, J.D., (2010). Experimental study of an inclined jet-in-cross-flow interacting with a vortex generator. 48th AIAA Aerospace Sciences Meeting, Orlando, Florida, 4–7 Jan. https://ntrs.nasa.gov/api/citations/20110016116/downloads/20110016116.pdf.

Zaman, K.B.M.Q., Rigby, D.L. and Heidmann, J.D., (2010). Inclined jet in crossflow interacting with a vortex generator. Journal of Propulsion and Power, 26(5), pp.947–954. https://doi.org/10.2514/1.49742.

Zhang, C. et al., (2020). Experimental and numerical study on the flat-plate film cooling enhancement using the vortex generator downstream for the fan-shaped hole configuration. Journal of Turbomachinery, 142(3), p.031006. https://doi.org/10.1115/1.4046234.

Zhao, Z. et al., (2022). Large eddy simulation of compound angle film cooling with vortex generators. International Journal of Thermal Sciences, 178, 107611. https://doi.org/10.1016/j.ijthermalsci.2022.107611.

Zheng, K. et al., (2021). An experimental study on the improvements in the film cooling performance by an upstream micro-vortex generator. Experimental Thermal and Fluid Science, 127, 110410. https://doi.org/10.1016/j.expthermflusci.2021.110410.